

Electrohydrodynamic instability of a thin film of viscoelastic polymer underneath a lithographically manufactured mask

Lin Wu^{a,*}, Stephen Y. Chou^b

^a Department of Mechanical Engineering, University of Nebraska-Lincoln, Lincoln, NE 68588, USA

^b NanoStructure Laboratory, Department of Electrical Engineering, Princeton University, New Jersey, NJ 08544, USA

Received 14 August 2002; received in revised form 13 July 2004; accepted 28 September 2004

Abstract

The electrohydrodynamic instability of a thin film of initially static viscoelastic polymer under a mask is studied via a linear analysis. The conducting polymer film is separated from the mask by air. Under a normal electrical field, the initially flat polymer film self-assembles into well organized micro scale patterns. The driving force for the instability is an electrostatic force exerted on the free charges accumulated at the air–polymer interface. The electrical field is either applied externally or generated internally by the contact potentials at the interfaces of different materials. The system is unconditionally unstable. The elasticity of the polymer is found to destabilize the system. When the Deborah number is large enough, a resonant phenomenon appears as a result of the interaction between the two destabilizing mechanisms (the electrostatic force and the polymer elasticity). The resonance introduces two most unstable wave numbers, at which the growth rate of the disturbance is unbounded. The two most unstable wave numbers bifurcate at a minimum Deborah number, below which no resonance is found. The effects of the initial film thickness, the air gap thickness and the electrical properties of the conducting polymer on the instability are also investigated.

© 2004 Elsevier B.V. All rights reserved.

Keywords: Bifurcation; Electrohydrodynamic instability; Leaky dielectric model; Non-Newtonian; Resonance; Thin film; Viscoelastic instability

1. Introduction

Lithographically induced self-assembly (LISA) [1–3], is an electrohydrodynamic instability process, in which a thin layer of melted polymer (usually PMMA) self-assembles into well organized pillar arrays that bridge the lower substrate and the upper mask. In a typical LISA experimental setup, a thin layer of polymer is spin coated and dried onto a substrate with a uniform film thickness around 100 nm (Fig. 1a). A lithographically manufactured mask is placed at a specified distance (around 100 nm) above the substrate with an air gap (around 100 nm) in between the polymer and the mask (Fig. 1b). The spacing between the mask and the substrate is well controlled by spacers. The polymer is subsequently heated above its glass transition temperature, which is about

130 °C depending on its molecular weight. An electrical field, which is either applied externally or induced internally by the contact potentials at the interfaces of different materials with different working functions, is built up between the mask and the substrate. The electrostatic force exerted on the free mobile (or polarized) charges, which are accumulated at the air–polymer interface, sets the interface into tension. The system becomes unstable subject to infinitesimal disturbances. Under certain situations, the result of the instability is well organized and results in micrometer sized hexagonal pillar arrays that connect the substrate and the mask (Fig. 1c). Although the lateral sizes of the pillars are not exactly the same due to imperfections in the experimental setup, they are observed to be closely distributed around a single wavelength [1,3] and the pillars have steep walls. However under other situations, no organized pattern is observed, and there are only random modulation patterns at the air–polymer interface [3].

* Corresponding author.

E-mail address: linwu@unlserve.unl.edu (L. Wu).

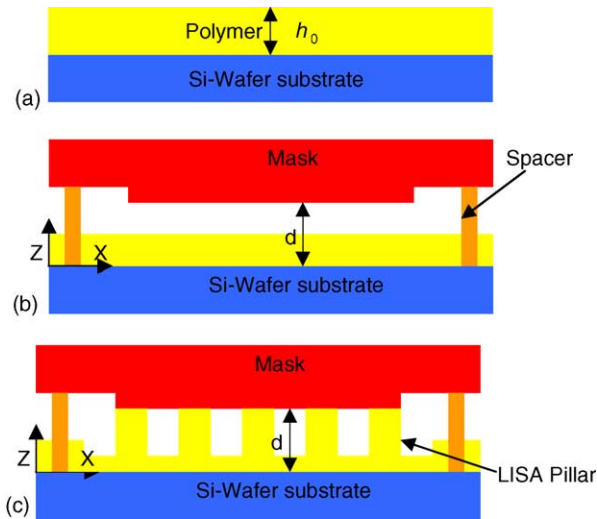


Fig. 1. The diagram of LISA experimental setup.

There were some instability studies on the LISA problem after its discovery due to its potential promising applications in electrical, optical and bioengineering devices [4–6]. According to these studies, the electrostatic force drives the instability and the surface tension force stabilizes the system. The air–polymer interface is always unstable subject to infinitesimal disturbances with a wave number ranging from zero to an upper bound, which has a value usually smaller than three (see the curve with a zero Deborah number in Fig. 3). Outside the single unstable domain, the system is stable to disturbances with all other wave numbers. Within the unstable domain, the positive growth rate changes smoothly and there is a most unstable wave number at which the positive growth rate is at its maximum. But a question arises immediately, why in some experiments do the pillars have very uniform size and well organized structures under certain situations? If the positive disturbance growth rate changes smoothly when the wave number changes from zero to an upper bound, we should always be able to find pillars with very different sizes. Or in another word, the resulting patterns should always be non-uniform and have no organized structures. It is one of our purposes to address this issue in this paper.

The previous studies [4–6] used some dielectric or leaky dielectric models to describe the electrical part of the problem. They assumed the fluid motion to be Newtonian. The non-Newtonian effect of the polymer melt was totally ignored. In this paper we want to investigate the effects of polymer elasticity on the instability. According to Pease and Russel's results [6], slight electrical conductivity of the polymer can significantly increase the disturbance growth exponent and reduces the fastest growing wavelength by a factor of 2–20. Since most polymers are conducting or weakly conducting, we implement the leaky dielectric model [7,8] to describe the electrical field part of the problem in a manner similar to Pease and Russel [6]. However we assume the fluid motion to be Non-Newtonian and obey the Oldroyd-

B constitutive equation [9]. The Oldroyd-B model is one of the simplest model capable of describing, at least qualitatively, the rheological behavior of dilute polymer solutions. By ignoring the viscous contribution from the solution, it can describe polymer melt flow. In our linear theory, we applied the lubrication assumption, i.e. the horizontal length scale is much larger than the vertical length scale. Under lubrication assumption, the elastic normal stresses are neglected in our linear theory due to the zero basic state solutions for the velocity and stress fields. The model thus reduces to the linear Jeffrey's model.

Our linear analysis shows that the polymer elasticity destabilizes the system and it increases the growth rate of disturbances. When the Deborah number is large enough, a resonant phenomenon appears as a result of the interaction of the electrostatic mode and the elastic mode. The resonance introduces two most unstable wave numbers, approaching each of which from only one side the growth rate becomes unbounded. The two wave numbers are observed to bifurcate at a minimum Deborah number, below which growth rate is increased by the elasticity but no resonant phenomenon is observed. The resonance phenomenon can explain why in some experiments only pillars with very uniform size and well organized patterns are observed [1], but in others the pillar size and patterns can be extremely irregular [3]. When the Deborah number is smaller than the minimum required value for resonance, the system is unstable for wave numbers distributed in a certain continuous range and the growth rate changes smoothly within that domain. Under this situation, the formed pillars can take an infinite number of sizes and the resulting patterns are extremely irregular. This makes the LISA process useless for industrial applications. When the Deborah number is larger than the minimum required value, resonance appears. As a result, only pillars with one resonant wave number are observed and the pillar patterns are extremely regular.

2. Governing equations and boundary conditions

We adopt a two-dimensional and one layer fluid model in the following analysis. The motion of air is totally ignored. Since the Reynolds number is very small, inertial effects are also ignored. Scarpulla et al.'s recent blow-off tests show that the flow of molecularly thin (a few nanometers thick) polymer above a solid surface can still be described by the continuum theory with the use of an enhanced effective viscosity [10]. The governing equations for the incompressible flow are the continuity equation and the Stokes equation:

$$\nabla \cdot \underline{u} = 0,$$

$$0 = -\nabla p + \nabla \cdot \underline{\underline{S}}, \quad (1)$$

where \underline{u} is the velocity vector with a component u in the x direction and a component w in the z direction (Fig. 2). The

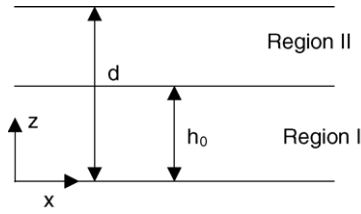


Fig. 2. The configuration of a thin layer of viscoelastic polymer under a mask. The polymer (region I) is separated from the mask by air (region II).

pressure is denoted p and \underline{S} is the stress tensor described by the Oldroyd-B constitutive equation [9]:

$$\underline{S} + \lambda^{(1)} \left(\frac{D\underline{S}}{Dt} - (\nabla \underline{u})^T \cdot \underline{S} - \underline{S} \cdot \nabla \underline{u} \right) = 2\eta_1 \left[\underline{D} + \lambda^{(2)} \left(\frac{D\underline{D}}{Dt} - (\nabla \underline{u})^T \cdot \underline{D} - \underline{D} \cdot \nabla \underline{u} \right) \right], \quad (2)$$

where $\underline{D} = \frac{1}{2}(\nabla \underline{u} + \nabla \underline{u}^T)$ is the rate of strain tensor. D/Dt is the substantive derivative. η_1 is the shear viscosity of the fluid. $\lambda^{(1)}$ and $\lambda^{(2)}$ are the relaxation time and the retardation time, respectively.

We implement the Taylor–Melcher leaky dielectrical model [7,8]. The magnetic field is ignored. The electrical fields in the polymer layer (with subscript I) and the air layer (with subscript II) obey the Maxwell equations:

$$\begin{aligned} \nabla \cdot (\varepsilon \varepsilon_0 \underline{E}_I) &= 0, \\ \nabla \times \underline{E}_I &= 0, \end{aligned} \quad (3a)$$

$$\begin{aligned} \nabla \cdot (\varepsilon_0 \underline{E}_{II}) &= 0, \\ \nabla \times \underline{E}_{II} &= 0, \end{aligned} \quad (3b)$$

where \underline{E}_I and \underline{E}_{II} are the electrical fields, and ε_0 and ε are the dielectric constants of the air and the polymer, respectively, which are assumed to be constant. Eq. (3a) and (3b) can be simplified into:

$$\nabla^2 \phi_I = 0, \quad (4a)$$

$$\nabla^2 \phi_{II} = 0, \quad (4b)$$

by introducing a potential function ϕ in each region with $\underline{E}_I = -\nabla \phi_I$ and $\underline{E}_{II} = -\nabla \phi_{II}$.

At the bottom wall ($z=0$) we apply no-slip and no-penetration boundary conditions:

$$u(0) = w(0) = 0. \quad (5)$$

At the air–polymer interface we have a dynamic interface condition:

$$w = \frac{\partial h}{\partial t} + u \frac{\partial h}{\partial x}, \quad (6)$$

where h is the height of the disturbed interface away from its initial position. Across the interface, the normal stresses are

balanced:

$$\begin{aligned} & \left(\llbracket -p \underline{I} + \underline{S} \rrbracket \cdot \underline{n} \right) \cdot \underline{n} + \frac{1}{2} \llbracket \varepsilon \varepsilon_0 (\underline{E} \cdot \underline{n})^2 - \varepsilon \varepsilon_0 (\underline{E} \cdot \underline{t})^2 \rrbracket \\ & + \gamma \frac{h_{xx}}{(1+h_x^2)^{3/2}} = 0, \end{aligned} \quad (7)$$

where \underline{n} and \underline{t} are the unit outside normal vector and the unit tangential vector of the interface, respectively. γ is the surface tension coefficient. $\llbracket \cdot \rrbracket$ denotes the “region II–region I” jump of the enclosed property across the interface. The tangential stresses are also balanced across the interface:

$$\left(\llbracket -p \underline{I} + \underline{S} \rrbracket \cdot \underline{n} \right) \cdot \underline{t} + q \underline{E} \cdot \underline{t} = 0, \quad (8)$$

where q is the area charge density at the interface, which is decided by a jump of the electrical field in the normal direction at the interface:

$$\llbracket \varepsilon \varepsilon_0 \underline{E} \rrbracket \cdot \underline{n} = q. \quad (9)$$

The charges at the interface are conserved and satisfy:

$$\frac{\partial q}{\partial t} + \underline{u} \cdot \nabla_s q = q \underline{n} \cdot (\underline{n} \cdot \nabla) \underline{u} + \llbracket -\sigma \underline{E} \cdot \underline{n} \rrbracket, \quad (10)$$

where ∇_s is the surface gradient and σ is the electrical conductivity.

At the polymer–substrate, air–polymer and mask–air interfaces, we assume constant electrical potential jumps:

$$\phi_I(0) = \Delta \phi_0, \quad (11a)$$

$$\phi_{II}(h) = \phi_I(h) + \Delta \phi_h, \quad (11b)$$

$$\phi_{II}(d) = -\Delta \phi_d, \quad (11c)$$

where $\Delta \phi_0$, $\Delta \phi_h$ and $\Delta \phi_d$ are potential jumps at $z=0$, $z=h$ and $z=d$, respectively. Their values are decided by the properties of the materials across the interface. In Eq. (11a)–(11c), we assume that the substrate and the mask are grounded.

3. Basic state solutions

The basic state solutions of the fluid part are very simple. For an initially static liquid polymer layer with a flat air–polymer interface, we have:

$$\hat{u} = \hat{w} = 0,$$

$$\hat{S}_{xx} = \hat{S}_{xz} = \hat{S}_{zz} = 0, \quad (12)$$

where \hat{S}_{xx} , \hat{S}_{xz} and \hat{S}_{zz} are three components of the tensor \underline{S} .

The solutions to Eq. (4a) and (4b), subject to boundary conditions (11a)–(11c), are:

$$\hat{\phi}_I(z) = \Delta \phi_0 - E_{Iz} z, \quad (13)$$

$$\hat{\phi}_{II}(z) = -\Delta \phi_d + E_{II}(d - z), \quad (14)$$

where E_I and E_{II} are the allowed constant electrical fields in region I and region II, respectively. At the polymer–substrate interface, Eq. (10) reduces to:

$$\frac{\partial \hat{q}}{\partial t} = -\sigma_I E_I \cdot e_z. \quad (15)$$

Since the polymer is conducting, $\sigma_I \neq 0$ for the polymer. To avoid a continued accumulation of charges at the polymer–substrate interface, we must have:

$$E_I = 0 \quad (16)$$

A similar argument does not hold at the mask–air interface because air is not conducting and $\sigma_{II} = 0$ holds. Substituting Eqs. (13), (14) and (16) into Eq. (11b) yields:

$$E_{II} = \frac{\Delta\phi}{d - h_0}, \quad (17)$$

where $\Delta\phi = \Delta\phi_0 + \Delta\phi_h + \Delta\phi_d$ is the total electrical potential jump. As a result, we have:

$$\hat{\phi}_I = \Delta\phi_0, \quad (18)$$

$$\hat{\phi}_{II} = -\Delta\phi_d + \frac{\Delta\phi}{d - h_0}(d - z). \quad (19)$$

The air–polymer interfacial charge density is obtained by substituting Eqs. (16) and (17) into Eq. (9):

$$\hat{q} = \frac{\varepsilon_0 \Delta\phi}{d - h_0}. \quad (20)$$

The pressure is obtained from the normal stress balance condition (7):

$$\hat{p} = -\frac{1}{2}\varepsilon_0 \left(\frac{\Delta\phi}{d - h_0} \right)^2. \quad (21)$$

4. The linearized perturbation equations and solutions

From the governing equations and the basic state solutions, we can identify the following characteristic scales: L for the horizontal length, d for the vertical length, U for the horizontal velocity, W for the vertical velocity, $\Delta\phi$ for the electrical field potential, $\Delta\phi/d$ for the electrical field strength, $\varepsilon_0 \Delta\phi/d$ for the charge density, $\varepsilon_0 \frac{\Delta\phi^2}{d^2}$ for the pressure. From the continuity equation, we have $\bar{W} \sim Ud/L$. Because of the zero basic state velocities and shear stresses, the constitutive Eq. (2) suggests: $S_{xz} \sim \eta_1 U/d$, $S_{xx} \sim \eta_1 U/L$, $S_{zz} \sim \eta_1 W/d = \eta_1 U/L$ and the time scale $T \sim d/W = L/U$. The choosing of the scale $S_{xx} \sim \eta_1 U/L$ needs more detailed discussion after we derive the linearized perturbation equation and introduce the normal modes. The horizontal length scale $L \sim \gamma^{1/2} d^{3/2} / \varepsilon_0^{1/2} \Delta\phi$ is determined by the balance of the electrostatic term and the surface tension term in the normal stress balance condition (7). The horizontal velocity scale $U \sim \varepsilon_0 \Delta\phi^2 / L \eta_1 = \varepsilon_0^{3/2} \Delta\phi^3 / \eta_1 \gamma^{1/2} d^{3/2}$ is determined by

the balance of the horizontal pressure gradient term $\frac{\partial p}{\partial x}$ and the shear stress gradient term $\frac{\partial S_{xz}}{\partial z}$ in the horizontal momentum equation.

For the current problem, the experimentally observed polymer structures due to the instability have a horizontal dimension ($\sim 10 \mu\text{m}$) much larger than the vertical dimension ($\sim 100 \text{nm}$). Thus, we have the lubrication condition $L \gg d$. The characteristic scales above are used to normalize the governing equations and boundary conditions (hereafter, all quantities are dimensionless).

To obtain the linearized perturbation equations, as usual we decompose each quantity f into a basic state quantity \hat{f} and a perturbation quantity \bar{f} :

$$f = \hat{f} + \bar{f}. \quad (22)$$

After substituting the decomposition of each of the unknowns into the governing equations and boundary conditions and keeping only the linear terms of the perturbation quantities and ignoring terms with a $O(d/L)$ or smaller magnitude (since d/L is a very small value), we obtain the linearized perturbation governing equations:

$$\frac{\partial \bar{u}}{\partial x} + \frac{\partial \bar{w}}{\partial z} = 0, \quad (23)$$

$$0 = -\frac{\partial \bar{p}}{\partial x} + \frac{\partial \bar{S}_{xz}}{\partial z}, \quad (24)$$

$$0 = -\frac{\partial \bar{p}}{\partial z}, \quad (25)$$

$$\bar{S}_{xz} + De \frac{\partial \bar{S}_{xz}}{\partial t} = \frac{\partial \bar{u}}{\partial z} + \delta De \frac{\partial^2 \bar{u}}{\partial t \partial z}, \quad (26)$$

$$\frac{\partial^2 \bar{\phi}_I}{\partial z^2} = 0, \quad (27)$$

$$\frac{\partial^2 \bar{\phi}_{II}}{\partial z^2} = 0, \quad (28)$$

where $De = \lambda^{(1)} U/L$ is the Deborah number [11] and $\delta = \lambda^{(2)}/\lambda^{(1)}$ is the ratio of the solvent viscosity to the shear viscosity.

For fluid part boundary conditions, we have:

$$\bar{u}(0) = \bar{w}(0) = 0. \quad (29)$$

At the air–polymer interface $Z = H_0$, we have:

$$\bar{w} = \frac{\partial \bar{h}}{\partial t}, \quad (30)$$

$$\bar{p} - \frac{1}{1 - H_0} \frac{\partial \bar{\phi}_{II}}{\partial z} + \bar{h}_{xx} = 0, \quad (31)$$

$$-\bar{S}_{xz} - \frac{1}{1 - H_0} \frac{\partial \bar{\phi}_{II}}{\partial x} + \frac{1}{(1 - H_0)^2} \frac{\partial \bar{h}}{\partial x} = 0. \quad (32)$$

For electrical boundary conditions, at $Z = H_0$, we have:

$$\varepsilon \frac{\partial \bar{\phi}_I}{\partial z} - \frac{\partial \bar{\phi}_{II}}{\partial z} = \bar{q}, \quad (33)$$

$$\frac{\partial \bar{q}}{\partial t} = \frac{1}{1 - H_0} \frac{\partial \bar{w}}{\partial z} - s \frac{\partial \bar{\phi}_I}{\partial z}, \quad (34)$$

where $s = \sigma_1 L / \varepsilon_0 U$ is the dimensionless conductivity, which has a value ranging from 10^3 to 10^{13} depending on the conductivity of the polymer under the actual experimental condition. We also have:

$$\bar{\phi}_I(0) = 0, \quad (35)$$

$$\bar{\phi}_I(H_0) = \bar{\phi}_{II}(H_0) - \frac{1}{1 - H_0} \bar{h}. \quad (36)$$

$$\bar{\phi}_{II}(1) = 0. \quad (37)$$

Since all coefficients in the governing equations and boundary conditions are constant, the following normal mode decomposition is adopted for each variable to transform the system into a set of linear ordinary differential equations:

$$\bar{f} = \tilde{f}(z) \exp(i\alpha(x - ct)), \quad (38)$$

where $\tilde{f}(z)$ is the amplitude function, α is the wave number normalized by $2\pi/L$ and c is the modified growth rate, which is a complex number. A positive imaginary part of c represents an unstable system, and a negative imaginary part of c represents a stable system.

To obtain Eq. (24), we assumed that the stress component S_{xx} scales as $\eta_1 U/L$. In fact, if the constitutive equation for the S_{xx} component (Eq. (2)) is normalized by all the chosen scales, the dominant terms are: $2\lambda^{(1)} \frac{\partial u}{\partial z} S_{zx} \sim \frac{\lambda^{(1)} \eta_1 U^2}{d^2}$ and $2\eta_1 \lambda^{(2)} \left(\frac{\partial u}{\partial z} \right)^2 \sim \frac{\lambda^{(2)} \eta_1 U^2}{d^2}$, which have a magnitude larger than $\eta_1 U/L$ when the Deborah number is $O(1)$. If we choose the scale of S_{xx} to be $\frac{\lambda^{(1)} \eta_1 U^2}{d^2}$ instead of $\eta_1 U/L$, the linearized perturbation equation for \tilde{S}_{xx} becomes:

$$\tilde{S}_{xx} + De \frac{\partial \tilde{S}_{xx}}{\partial t} = 0,$$

which has admissible solutions $\tilde{S}_{xx} = 0$ or $i\alpha c = \frac{1}{De}$. The solution $i\alpha c = \frac{1}{De}$ represents a stable mode that is not compatible with other perturbation equations and boundary conditions and should be dropped. The only valid solution $\tilde{S}_{xx} = 0$ validates our assumption that S_{xx} has a magnitude much smaller than S_{xz} under the lubrication condition $L \gg d$. As a result, for linear analysis, $S_{xx} \sim \eta_1 U/L$ is a valid scaling and the normal stresses S_{xx} and S_{zz} are negligible compared with the shear stress S_{xz} in our linear theory due to the zero basic state solutions for the velocity and stress fields.

To further simplify the problem, we introduce a perturbation stream function ψ so that:

$$(\tilde{u}, \tilde{w}) = (\psi', -i\alpha\psi). \quad (39)$$

After substituting the normal modes (Eq. (38)) and the stream function (Eq. (39)) into the dimensionless governing equations and boundary conditions and eliminating the pressure (and after dropping all \sim for simplicity), we obtain the governing equations:

$$S''_{xz} = 0, \quad (40)$$

$$(1 - iDe\alpha c)S_{xz} = (1 - i\delta De\alpha c)\psi'', \quad (41)$$

$$\phi_I'' = 0, \quad (42)$$

$$\phi_{II}'' = 0, \quad (43)$$

and the boundary conditions:

$$\psi(0) = \psi'(0) = 0, \quad (44)$$

$$\psi(H_0) = ch, \quad (45)$$

$$S'_{xz}(H_0) - \frac{i\alpha}{1 - H_0} \phi_{II}'(H_0) - i\alpha^3 h = 0, \quad (46)$$

$$-S_{xz}(H_0) - \frac{i\alpha}{1 - H_0} \phi_{II}(H_0) + \frac{i\alpha}{(1 - H_0)^2} h = 0, \quad (47)$$

$$\varepsilon \phi_I'(H_0) - \phi_{II}'(H_0) = q, \quad (48)$$

$$i\alpha c q = \frac{i\alpha}{1 - H_0} \psi'(H_0) + s \phi_I'(H_0), \quad (49)$$

$$\phi_I(0) = 0, \quad (50)$$

$$\phi_I(H_0) = \phi_{II}(H_0) - \frac{1}{1 - H_0} h, \quad (51)$$

$$\phi_{II}(1) = 0. \quad (52)$$

To obtain the amplitude functions of the electrical potential function, we can directly integrate Eqs. (42) and (43) by using boundary conditions (48), (50)–(52) to yield:

$$\phi_I = \left(\frac{1 - H_0}{H_0 - \varepsilon(H_0 - 1)} q - \frac{1}{(1 - H_0)(H_0 - \varepsilon(H_0 - 1))} h \right) z, \quad (53)$$

$$\begin{aligned} \phi_{II} = & - \left(\frac{H_0}{H_0 - \varepsilon(H_0 - 1)} q \right. \\ & \left. + \frac{\varepsilon}{(1 - H_0)(H_0 - \varepsilon(H_0 - 1))} h \right) (z - 1). \end{aligned} \quad (54)$$

The shear stress is obtained by integrating Eq. (40) subject to boundary conditions (46) and (47):

$$\begin{aligned} S_{xz} = & \left(\frac{-i\alpha H_0}{(1 - H_0)(H_0 - \varepsilon(H_0 - 1))} q + \left(\frac{-i\alpha \varepsilon}{(1 - H_0)^2 (H_0 - \varepsilon(H_0 - 1))} + i\alpha^3 \right) h \right) Z + \frac{i\alpha H_0 (2H_0 - 1)}{(1 - H_0)(H_0 - \varepsilon(H_0 - 1))} q \\ & + \left(\frac{i\alpha \varepsilon (2H_0 - 1)}{(1 - H_0)^2 (H_0 - \varepsilon(H_0 - 1))} - i\alpha^3 H_0 + \frac{i\alpha}{(1 - H_0)^2} \right) h. \end{aligned} \quad (55)$$

The stream function is obtained by integration of Eq. (41) after we substitute the solution of the shear stress into it and use the boundary condition (44). At position $z=H_0$, we have:

$$\psi(H_0) = i\alpha \frac{1 - i\alpha Dec}{1 - i\alpha De\delta c} (a_1 q + a_2 h), \quad (56)$$

where

$$a_1 = \frac{5H_0^4 - 3H_0^3}{6(1 - H_0)(H_0 - \varepsilon(H_0 - 1))},$$

$$a_2 = \frac{5\varepsilon H_0^3 - 3\varepsilon H_0^2}{6(1 - H_0)^2(H_0 - \varepsilon(H_0 - 1))} - \frac{1}{3}\alpha^2 H_0^3 + \frac{H_0^2}{2(1 - H_0)^2}. \quad (57)$$

We also have

$$\psi'(H_0) = i\alpha \frac{1 - i\alpha Dec}{1 - i\alpha De\delta c} (\beta_1 q + \beta_2 h), \quad (58)$$

where

$$\beta_1 = \frac{3H_0^3 - 2H_0^2}{2(1 - H_0)(H_0 - \varepsilon(H_0 - 1))}, \quad (59)$$

$$\beta_2 = \frac{3\varepsilon H_0^2 - 2\varepsilon H_0}{2(1 - H_0)^2(H_0 - \varepsilon(H_0 - 1))} - \frac{\alpha^2 H_0^2}{2} + \frac{H_0}{(1 - H_0)^2}. \quad (60)$$

Above solutions together with boundary conditions (45) and (49) form an eigenvalue problem with the modified growth rate c being the eigenvalue of the system, which obeys the 4th order complex algebra equation:

$$(i\alpha a_2 + (\alpha^2 De a_2 - 1)c + i\alpha De \delta c^2) (b_1 + c_1 - i\alpha(De b_1 + De c_1 \delta - 1)c + \alpha^2 De \delta c^2) - (i\alpha a_1 + \alpha^2 a_1 De c)(b_2 + c_2 - i\alpha De (b_2 + \delta c_2)c) = 0, \quad (61)$$

where

$$(b_1, b_2) = \frac{\alpha^2}{(1 - H_0)} (\beta_1, \beta_2), \quad (62a)$$

and

$$c_1 = -\frac{s(1 - H_0)}{H_0 - \varepsilon(H_0 - 1)},$$

$$c_2 = \frac{s}{(1 - H_0)(H_0 - \varepsilon(H_0 - 1))}. \quad (62b)$$

For polymer melt, $\delta=0$, Eq. (61) is further simplified into:

$$iN_I + N_{III}c - iN_{III}c^2 = 0, \quad (63)$$

where

$$N_I = \alpha(a_1 b_2 + a_1 c_2 - a_2 b_1 - a_2 c_1), \quad (64)$$

$$N_{II} = (2a_1 b_2 + a_1 c_2 - 2a_2 b_1 - a_2 c_1)\alpha^2 De + \alpha^2 a_2 + b_1 + c_1, \quad (65)$$

$$N_{III} = (a_1 b_2 - a_2 b_1)\alpha^3 De^2 + (\alpha^3 a_2 + \alpha b_1)De - \alpha. \quad (66)$$

The modified growth rate is a complex number:

$$c = c_R + i c_I. \quad (67)$$

A positive imaginary part c_I corresponds to an unstable system. The real part of Eq. (63) yields:

$$c_R(2N_{III}c_I + N_{II}) = 0. \quad (68)$$

For one solution (standing wave solution):

$$c_R = 0, \quad (69)$$

we obtain

$$c_I = \frac{-N_{II} \pm \sqrt{N_{II}^2 - 4N_I N_{III}}}{2N_{III}}. \quad (70)$$

For another solution (traveling wave solution)

$$c_I = -\frac{N_{II}}{2N_{III}}, \quad (71)$$

we obtain

$$c_R = \pm \sqrt{\frac{N_I + N_{II}c_I + N_{III}c_I^2}{N_{III}}} = \pm \sqrt{\frac{4N_I N_{III} - N_{II}^2}{4N_{III}}}. \quad (72)$$

5. Results and discussions

From the solutions we find that there are several important parameters and dimensionless groups (the dimensionless polymer film thickness H_0 , the dielectric constant of the polymer ε , the dimensionless conductivity of the polymer s , the Deborah number De and dimensionless wave number α) for the results. Fig. 3 plots the growth rate αc_I as a function of wave number for different Deborah numbers for the case $H_0=0.3$, $\varepsilon=2$, $s=1000$. The system is always unstable

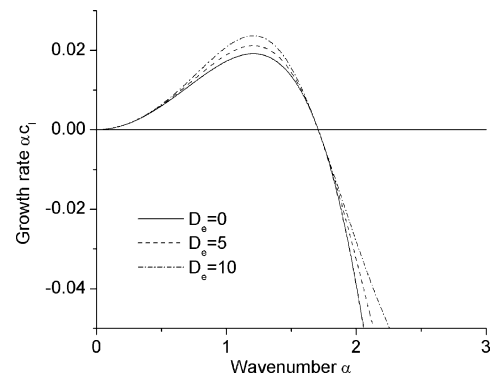


Fig. 3. The growth rate as a function of wave number α for different Deborah number De with $H_0=0.3$, $\varepsilon=2$, $s=1000$, $\delta=0$.

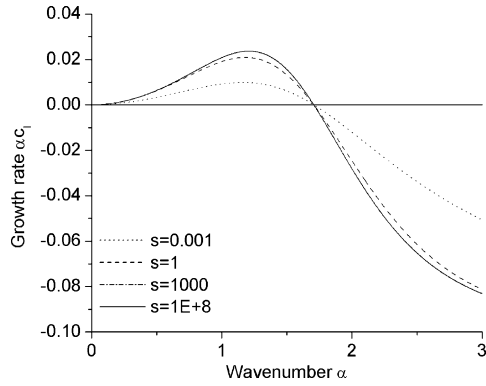


Fig. 4. The growth rate as a function of wave number α for different dimensionless conductivity s with $H_0=0.3$, $\varepsilon=2$, $De=10$, $\delta=0$.

with a most unstable wave number around 1.32. The unconditional instability at long wavelength is due to the nature of the driving force (electrostatic force) and the stabilizing force (surface tension). If the initially flat interface is disturbed, the electrostatic suction force on the peak of the disturbed interface is increased. The higher the peak rises, the stronger the suction force becomes. The electrostatic force does not depend that much on the wavelength. However, at long wavelength, the surface tension is weak. The combined result is an instability at long wavelength. When the wavelength is decreased, the surface tension force stabilizes the system as expected. Fig. 3 also shows that the polymer elasticity destabilizes the system. The growth rate increases with the Deborah number. The elasticity does not shift the most dangerous wave number.

Fig. 4 plots the growth rate αc_1 corresponding to different dimensionless conductivities for fixed $H_0=0.3$, $\varepsilon=2$, and $De=10$. Similar to the Newtonian study [6], increasing the conductivity by several orders of magnitude only slightly increases both the growth rate and the most dangerous wave number for a conducting polymer. The difference between a perfect dielectric polymer and a weakly conducting polymer was found to have a significant effect on the instability for the Newtonian case [6]. We assume that similar conclusion holds for Non-Newtonian case, even though in this paper we only consider conducting polymers.

In Fig. 5, we increase the film thickness to 0.5 but keep $\varepsilon=2$ and $s=1000$. When the Deborah number is below 1.677, the elasticity increases the growth rate αc_1 without shifting the most dangerous wave number. But when the Deborah number is equal to or larger than 1.677, a resonant phenomenon appears. The resonance corresponds to an infinitely large growth rate. For the case $De=1.68$, the resonance happens at two wave numbers $\alpha=1.924$ and 2.004 . The growth rate approaches infinity as the wave number approaches $\alpha=1.924$ from the left and $\alpha=2.004$ from the right. In between, the growth rate is negative and the system is stable.

Fig. 6 plots the growth rate αc_1 of the three different modes (Eqs. (70) and (71)) for the case $H_0=0.5$, $\varepsilon=2$, $De=1.4$ and $s=1000$. The g_{1+} and g_{1-} modes correspond to Eq. (70) with

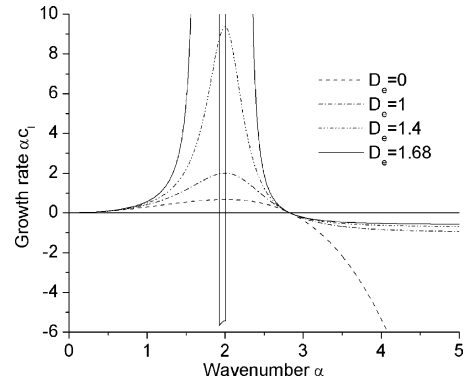


Fig. 5. The growth rate as a function of wave number α for different Deborah number De with $H_0=0.5$, $\varepsilon=2$, $s=1000$, $\delta=0$.

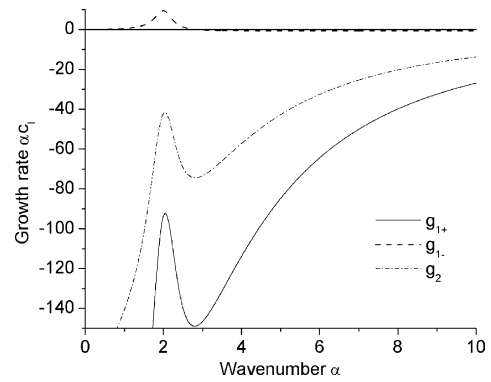


Fig. 6. The growth rate as a function of wave number α for different modes with $De=1.4$ and $H_0=0.5$, $\varepsilon=2$, $s=1000$, $\delta=0$. All curves approach an asymptotic value -0.7143 as $\alpha \rightarrow \infty$.

a plus and a negative signs, respectively. The g_2 mode corresponds to Eq. (71). All three modes approach an asymptotic value -0.7143 as $\alpha \rightarrow \infty$.

Fig. 7 plots the three modes of αc_1 for the case $H_0=0.5$, $\varepsilon=2$, $De=1.68$ and $s=1000$. The g_{1+} mode is always stable, but the g_{1-} and the g_2 modes have resonance at $\alpha=1.924$ and 2.004 . g_{1-} corresponds to a standing wave mode and g_2 corresponds to a traveling wave mode.

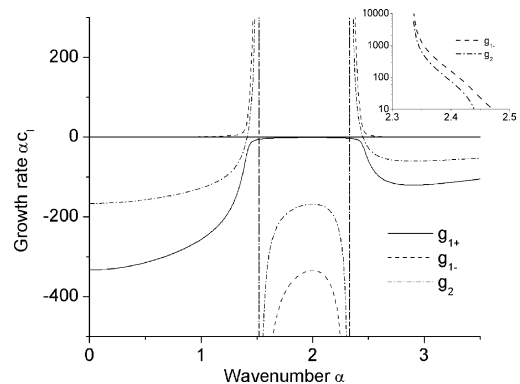


Fig. 7. The growth rate as a function of wave number α for different modes with $De=2$ and $H_0=0.5$, $\varepsilon=2$, $s=1000$, $\delta=0$. The inset shows the g_{1-} and g_2 modes near the right hand side resonance point.

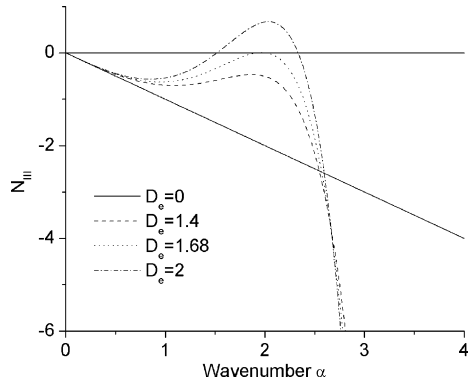


Fig. 8. N_{III} as a function of wave number α for different Deborah number De with $H_0=0.5$, $\varepsilon=2$, $s=1000$, $\delta=0$.

The resonance happens at wave numbers that are singular points of Eq. (63) (zero N_{III} at $\alpha \neq 0$). N_{III} is always equal to zero at $\alpha=0$ (see Eq. (66)). However, $\alpha=0$ is not a singular point because we have $c_1=0$ at $\alpha=0$. N_{III} is a negative value when the Deborah number is equal to zero and $\alpha>0$. As a result, resonance phenomenon is impossible for the case with a zero Deborah number. Nevertheless, when the Deborah number is large enough, N_{III} may have zero value at one or two non-zero wave numbers α , which induces the resonance phenomenon. Fig. 8 plots N_{III} as a function of wave number α for different Deborah numbers with fixed $H_0=0.5$, $\varepsilon=2$ and $s=1000$. When the Deborah number is less than 1.677, N_{III} is always negative and there is no resonance. When the Deborah number is above 1.677, it has two zero points in addition to the long wave limit $\alpha=0$ (not a resonance point), and the separation of the two zero points increases with the Deborah number.

Fig. 9 shows that for the case $H_0=0.5$, $\varepsilon=2$ and $s=1000$, $(N_I + N_{II}c_1 + N_{III}c_1^2)/N_{III}$ is negative for all wave numbers smaller than 5, which means that the traveling wave solutions (Eqs. (71) and (72)) are not valid for all the Deborah numbers considered if the wave number is smaller than 5. The reason is that c_R should be real because we already divided the complex eigenvalue into a real and an imaginary part $c = c_R + ic_I$. Both c_R and c_I are real values. But the travelling wave solution

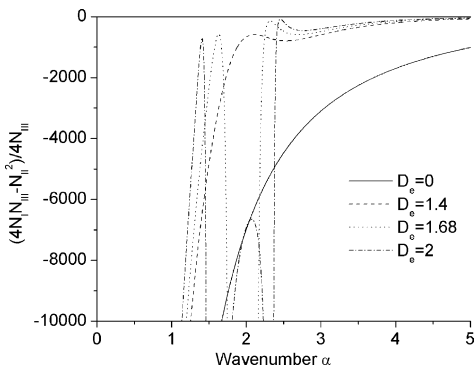


Fig. 9. c_R^2 (in Eq. (71)) as a function of wave number α for different Deborah number De with $H_0=0.5$, $\varepsilon=2$, $s=1000$, $\delta=0$.

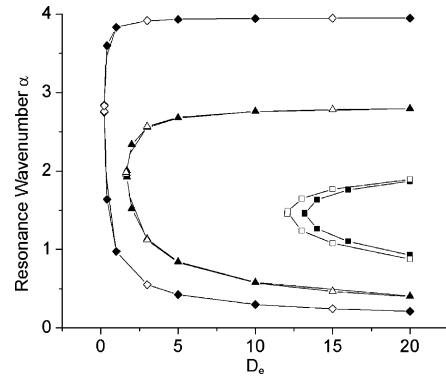


Fig. 10. The resonant wave number α as a function of Deborah number De for different H_0 and ε ($s=1000$, $\delta=0$ for all cases). Curves with similar marks (solid or open) have the same H_0 value: square, $H_0=0.4$; triangle, $H_0=0.5$; diamond, $H_0=0.6$. Solid marks correspond to $\varepsilon=2$ and open marks correspond to $\varepsilon=3.6$.

$c_R \neq 0$ corresponds to $c_R^2 < 0$, which means c_R is imaginary. As a result, the standing wave modes Eqs. (69) and (70) are the only valid solutions. The same conclusion holds for all cases studied in this paper.

Fig. 10 plots the resonant wave numbers as a function of the Deborah number for different dimensionless polymer film thickness and different dielectric constant of the polymer. Resonance happens only when the Deborah number is larger than a minimum value, above which the resonance wave number bifurcates into two branches, and below which no resonance will happen. The two resonance wave numbers quickly approach their asymptotic values as the Deborah number increases. Fig. 10 indicates that the resonance phenomenon is very sensitive to the initial dimensionless film thickness. A smaller dimensionless film thickness makes it more difficult to achieve resonance and requires larger Deborah number to trigger the resonance. A slight change in the dimensionless film thickness from 0.4 to 0.5 decreases the minimum resonance Deborah number by 10 and more than doubles the difference between the two resonance wave numbers. When the dimensionless film thickness is larger than 0.5, only a very small Deborah number is needed to induce the resonance phenomenon. The difference between the two resonant wave numbers also increases with the dimensionless film thickness. Fig. 10 also shows that the resonance phenomenon is not sensitive to the dielectric constant of the polymer. The dielectric constant has a large effect on the resonance wave numbers when the dimensionless film thickness is small. When the dimensionless film thickness H_0 is equal to 0.5 and 0.6, the difference between the curve $\varepsilon=2$ (with solid marks) and the curve $\varepsilon=3.6$ (with open marks) is so small that the two curves almost overlap. A noticeable difference is observed only at the beginning of the bifurcation when H_0 is decreased to 0.4. But the difference disappears quickly as the two wave numbers approach their asymptotic values when the Deborah number is increased. From the definition of N_{III} , we notice that the conductivity of the polymer s has no effect on the resonance.

For a typical experimental system setup with the PMMA polymer being used, we have the following estimations for the magnitude of the physical parameters: $d \sim 10^{-7}$ m, $\Delta\phi \sim 1$ V, $\gamma \sim 0.03$ N/m, $\eta_1 \sim 100$ Pa s, $\varepsilon_0 = 8.85 \times 10^{-12}$ C²/N m. Subsequently, we can calculate the horizontal length scale $L = \gamma^{1/2} d^{3/2} / \varepsilon_0^{1/2} \Delta\phi \approx 2 \times 10^{-6}$ m and the velocity scale $U = \varepsilon_0^{3/2} \Delta\phi^3 / \eta_1 \gamma^{1/2} d^{3/2} \approx 4 \times 10^{-8}$ m/s. As a result, we have $L \gg d$. The lubrication assumption is validated. For the resonance phenomenon to happen, we have $De = \lambda^{(1)} U / L \approx 1$, which requires an average relaxation time $\lambda^{(1)} \sim 50$ s, a value that is within the reasonable range of PMMA polymer's rheology properties. For the case $H_0 = 0.5$ and $\varepsilon = 2$, the larger resonance wave number is $\alpha = 2.7$, which results in a LISA pillar period $\lambda \sim 5$ μ m. Our prediction agrees well with the experimental observations.

6. Conclusions

In this paper, we have investigated the non-Newtonian effect of the polymer melt on the electrohydrodynamic instability of a thin polymer film underneath a lithographically manufactured mask. We find that the viscoelasticity plays a significant role in the instability process. The polymer elasticity destabilizes the system. A resonance phenomenon is discovered when the viscoelasticity is large enough. The resonance is found to be sensitive to the dimensionless film thickness

of the polymer but not sensitive to the electrical properties of the polymer layer.

References

- [1] S.Y. Chou, L. Zhuang, Lithographically induced self-assembly of periodic polymer micropillar arrays, *J. Vac. Sci. Technol.*, B 17 (1999) 3197.
- [2] S.Y. Chou, L. Zhuang, L. Guo, Lithographically induced self-construction of polymer microstructures for resistless patterning, *Appl. Phys. Lett.* 75 (1999) 1004.
- [3] E. Schaffer, T. Thurn-Albrecht, T.P. Russell, U. Steiner, Electrically induced structure formation and pattern transfer, *Nature* 403 (2000) 874.
- [4] E. Schaffer, T. Thurn-Albrecht, T.P. Russell, U. Steiner, Electrohydrodynamic instability in polymer films, *Europhys. Lett.* 53 (2001) 518.
- [5] Z. Suo, J. Liang, Theory of lithographically-induced self-assembly, *Appl. Phys. Lett.* 78 (2001) 3971.
- [6] L.F. Pease, W.B. Russel, Linear stability analysis of thin leaky dielectrical films subject to electrical fields, *J. Non-Newtonian Fluid Mech.* 102 (2002) 233.
- [7] G.I. Taylor, The stability of a horizontal fluid interface in a vertical electrical field, *J. Fluid Mech.* 22 (1965) 1.
- [8] D.A. Saville, Electrohydrodynamics: the Taylor–Melcher leaky dielectrical model, *Annu. Rev. Fluid Mech.* 29 (1997) 27.
- [9] R.G. Larson, *Constitutive Equations for Polymer Melts and Solutions*, Butterworth, Stoneham, MA, 1988.
- [10] M.A. Scarpulla, C.M. Mate, M.D. Carter, Air shear driven flow of thin perfluoropolyether films, *J. Chem. Phys.* 94 (2003) 3368.
- [11] R.B. Bird, R.C. Armstrong, O. Hassager, *Dynamics of polymeric liquids*, Fluid Mechanics, vol. 1, Wiley, New York, 1987.